PHYSICAL REVIEW B **82**, 235314 (2010)

Charged excitons and biexcitons in laterally coupled (In,Ga)As quantum dots

Jie Peng and Gabriel Bester*
Max-Planck-Institut für Festkörperforschung, Heisenbergstr. 1, D-70569 Stuttgart, Germany
(Received 17 August 2010; published 13 December 2010)

We present results of atomistic empirical pseudopotential calculations and configuration interaction for excitons, positive and negative trions ($X^{\pm}$), positive and negative quartons ($X^{2\pm}$), and biexcitons. The structures investigated are laterally aligned InGaAs quantum dot molecules embedded in GaAs under a lateral electric field. The rather simple energetic of excitons becomes more complex in the case of charged quasiparticles but remains tractable. The negative trion spectrum shows four anticrossings in the presently available range of fields while the positive trion shows two. The magnitude of the anticrossings reveals many-body effects in the carrier tunneling process that should be experimentally accessible.

DOI: 10.1103/PhysRevB.82.235314 PACS number(s): 73.21.La, 78.67.Hc, 78.55.Cr, 71.35.−y

I. INTRODUCTION

Epitaxial semiconductor quantum dots (QDs) can be designed with an increasing degree of control over their sizes, shapes, and alloy compositions.[1,2] Individual structures can be arranged laterally and vertically using controlled self-assembly or substrate patterning, to generate complex arrangements of QDs. This newly gained ability to deterministically produce architectures of QDs is the prerequisite for the implementation of scalable quantum networks, where each QD holds a quantum bit (qubit). Furthermore, impressive advances were made in the manipulation of the realized quantum states; enabled by a fundamental understanding of the QDs electronic and optical properties. For single QDs, different types of quantum states were already manipulated. Early work focused on the coherent manipulation of exciton qubits,[3–8] but due to their rather short coherence times, the attention has shifted to the electron spin. The initial step of the single spin initialization was demonstrated[9–11] and is now part of more advanced spin manipulation experiments.[12–16]

For structures with more than one QD, the most advanced prototypes are vertically aligned (stacked) quantum dot molecules (QDMs). These structures have appeared more than a decade ago[17–19] but have developed into a fertile platform for quantum manipulations only recently. One important step was the fabrication of structures designed to allowing either electron or hole tunneling.[20] The observation of the coupling through anticrossings under vertical electric field[21–24] along with theoretical atomistic modeling[25–27] allowed for precise estimates of many relevant coupling energies. Indeed, the understanding of the quantum states in vertically coupled QDMs is rather deep and goes beyond coupling energies. For instance, the existence of an antibonding ground state[28,29] could be demonstrated, the influence of a lateral misalignment of the QDs was investigated[30] and indirect excitons could be recently observed.[31] Success in the area of *control* and *manipulation* was very recently reported for vertically stacked QDMs. Namely, the optical spin initialization over the fine structure of the excited trion state[11] and the ultrafast control of the entanglement between two electrons spins located in different dots.[32] This represents the first two-qubit operation with QDs.

The history of *laterally* aligned QDMs is younger with high-quality structures appearing only in the last few year.[1,2,33–36] Laterally coupled QDMs are certainly good candidates for applications in quantum information science because of the potential to couple several QDs ("scaling") to form the first building block of a useful device. It is also believed that the degree of external control of individual QDs within a QDM or an array of laterally aligned QDs should be larger than in vertical structures. However, the control until now has been limited due to the difficulty to apply lateral electric fields in order to gate (or tune) the device. Indeed, the geometrical constraints have lead to relatively weak[37,38] applied lateral fields until now. Likewise, the charging of the QDM with extra carriers, as achieved regularly in vertical structures through tunneling from a δ-doping layer, has not yet been achieved in lateral structures. These limitations are not believed to be of fundamental nature but certainly represent technical challenges.

Theoretical understanding of the lateral structures as grown in Ref. 2 was facilitated by a detailed experimental analysis of their morphology.[2] The recent agreement between theory and experiment[38–40] for the exciton problem is astonishing, simply using the composition profile, sizes, and shapes determined experimentally. However, the experimentally available range of fields did not give access to anticrossings but revealed the dot coupling through a switch of intensity between the exciton branch of one dot to the exciton branch of the other dot composing the QDM. The observed photoluminescence (PL) therefore shows coupling,[38] but its magnitude, which is possible to simply read out from anticrossings, remains experimentally unobserved in these type of dots. Our theoretical results[38] showed electronic coupling in the range of 0.6–1.1 meV and vanishing hole coupling. The simplicity in the energetic of the excitonic states allowed us to gain some insight into the carrier dynamic. The comparison theory-experiment leads us to derive a model where the photogenerated electron from the electron-hole pair enters the structure first and thermalizes into the lowest energy state, before the hole enters the structure to create a bound exciton. This model of a quick electron capture and thermalization will also be the base of the present investigations. It brings a whole new level of complexity to the modeling but is necessary to obtain meaningful field-dependent PL results.

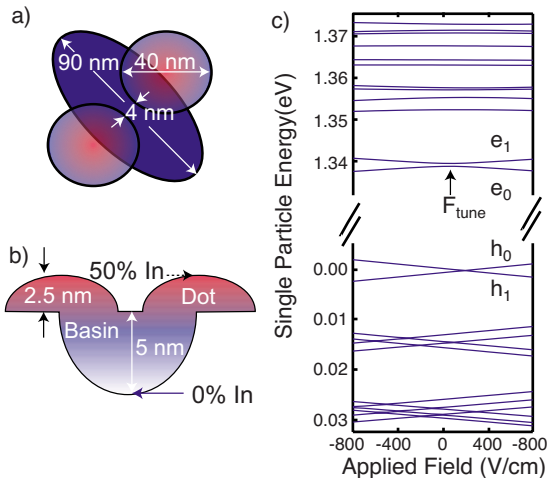

FIG. 1. (Color online) (a) Top view [(001) plane] and (b) cross-sectional view [(110) plane] of the two lens-shaped InGaAs dots and the basin embedded in GaAs. (c) Single-particle energies of the first 12-electron and first 12-hole states as a function of the lateral electric field.

We present a detailed analysis of charged exciton complex in laterally coupled InGaAs/GaAs QDMs. We describe the studied structure, the theoretical method, and then the single-particle results that build the basis for the calculation of the charged and biexciton states. We then discuss subsequently the negative and positive trion, the negative and positive quarton ($X^{2\pm}$), and the biexciton. For these species we present results for the photoluminescence taking dynamical processes of the quasiparticle formation into account. We predict the existence of four and two anticrossings within the experimentally available rang of fields and show that these contain valuable information on many-body tunneling effects.

II. STRUCTURE

The QDMs we are addressing are grown by molecular beam epitaxy and *in situ* atomic layer precise etching. This process leads to the creation of a low-density ensemble of InAs/GaAs double dots aligned along the $[1\bar{1}0]$ crystal axis.[37,41] The growth process is such that, a nanohole, referred to as "basin" in the following, is formed and subsequently overgrown to support the formation of two lens-shaped dots characterized in detail in Ref. 2. Details of the structure are given in Figs. 1(a) and 1(b) in a top and a side view of the structure. A linear composition gradient from the bottom of the basin (the filled hole) to the top of the dots is used throughout the structure. The basin is relatively deep, but has a low In concentration. Nevertheless the coupling of electronic states is facilitated by its presence. The dimensions given in Figs. 1(a) and 1(b) have been used for all the results presented here. However, we varied the dot separation between 0 and 8 nm, the dot diameters between 38 and 44 nm, allowing for dots of different sizes, and simulated a QDM with dots of dissimilar heights.[38] This variation in sizes follows the experimental characterization[2] and leads to small differences in the results. Astonishingly, the differences obtained following these size and shape variations are in the same order of magnitude as the ones obtained from two QDMs identical in their morphology but simply created from two different random alloys.[38] We will present results of two such QDMs that we labeled QDM0 and QDM5. They represent two different cases where the energetic splittings between the energy gap of the left and the right dots are small (QDM5) and large (QDM0).

III. THEORETICAL METHOD

We use the atomistic empirical pseudopotential approach[42,43] to obtain the single-particle eigenvectors as solution of the Schrödinger equation

$$\hat{H}\psi_i(\mathbf{r}) = \left\{ -\beta\frac{\nabla^2}{2} + V_{loc}^{\mathrm{EPM}}(\mathbf{r}) + \hat{V}_{\mathrm{SO}} \right\}\psi_i(\mathbf{r}) = \varepsilon_i\psi_i(\mathbf{r}), \quad (1)$$

using a basis set of strained Bloch function of the underlying bulk[42] with a low-energy cut-off of 5 Ry. The local empirical pseudopotential $V_{loc}^{\mathrm{EPM}}(\mathbf{r})$ is fitted to reproduce known experimental quantities such as the bulk band structure at high-symmetry points, the effective masses for different bands at different k points and along different reciprocal space directions, the deformation potentials and the surface work function. The potential has a strain-dependent term[43] and the spin-orbit potential $\hat{V}_{\mathrm{SO}}$ has one parameter that is fitted to reproduce experimental spin-orbit splittings. The kinetic energy is rescaled by the factor β, which enables us to fit both gap and effective masses nearly perfectly.[43] This method takes strain, band coupling, coupling between different parts of the Brillouin zone, and spin-orbit coupling into account, retaining the atomistically resolved structure. Hence, two structures with identical overall shapes and average compositions x are distinct, since each structure is the product of a process where the uncommon atoms (In and Ga) occupy their sites randomly but keeping an overall concentration of x.

The excitonic properties are calculated using the configuration interaction approach[44] with the two center integrals

$$\langle e_j h_i | v | h_{i'} e_{j'} \rangle \quad (2)$$

$$= \int\int \psi_j^*(\mathbf{r}_e)\psi_i^*(\mathbf{r}_h)v(\mathbf{r}_e,\mathbf{r}_h)\psi_{i'}(\mathbf{r}_e)\psi_{j'}(\mathbf{r}_h)d\mathbf{r}_e d\mathbf{r}_h, \quad (3)$$

using the Resta model for the screening function $v(\mathbf{r}_e,\mathbf{r}_h)$. A review of the method can be found in Ref. 43.

The many-body states are labeled according to Table I. In this labeling we use the dot-localized basis, in which the particles are well localized within one dot, either right (R) or left (L). This basis is not the natural basis from a computational point of view where the states are given in the "molecular" basis. In other words, the eigenfunctions of Eq. (1) would yield as lowest electron state a bonding state (see below) that we label e_0 and that can only be expressed as linear combination of dot-localized states (e_L+e_R). To give the results in the convenient dot-localized basis requires a

TABLE I. Key to the different abbreviations used to describe the excitonic species.

Name	Symbol	Labeling	Species
Exciton	X	*he*	LL RR LR
Negative trion	X^-	*hee*	LLL LLR RRR RRL (direct)
			LRR RLL (indirect)
Positive trion	X^+	*ehh*	Same as X^-
Negative quarton	X^{2-}	*heee*	LLLR LLRR RLLR RLRR
Positive quarton	X^{2+}	*ehhh*	Same as X^{2-}
Biexciton	XX	*hhee*	LLLL LLLR LRRR LRRL
			LRLL RRRR RRRL (direct)
			LLRR RRLL (indirect)

projection. Furthermore, the few-body states, we calculate by configuration interaction, are combinations of many different determinants, such as LL, LR, but also $e_i h_j$, where (i,j) can be excited states. The great simplification to the species from Table I should be seen as an *a posteriori* analysis of our many-body results.

IV. SINGLE-PARTICLE ENERGIES AND WAVE FUNCTIONS

The single-particle energies and square of the wave functions for the first 12-electron and first 12-hole states are given in Figs. 1(c) and 2 as a function of the applied lateral electric field applied along the $[1\bar{1}0]$ direction (positive fields point from the left to the right dot). The hole states form a shell-like structure with the two S states, four P states, and six D states, much like in the case of two large single dots. Note that for smaller dots with a larger aspect ratio (height/diameter), the hole states can show strong deviations from the shell structure shown here and acquire significant S-P mixing.[45] The electron states, on the other hand, show strong deviations from the shell structure familiar from single quantum dots. This is due to the existence of basin states that strongly hybridize with dotlike states. Most prominently in state e_2 in Fig. 2 the basin S state hybridizes with the dot P states. In state e_7 the dot P state and the basin P state hybridize. The symmetry of higher electron states deviates strongly from the symmetry of single dots and this affects the absorption spectrum in a significant manner.[40] This effect can also be seen on the almost vanishing slopes of the single-particle energy versus field in Fig. 1(c). However, the electron S states are energetically quite remote from the complications created by the basin states on the higher energy states (e_i with $i>1$) so that processes of emission, that typically involve the lowest few single-particle states only, will remain nearly unaffected by the basin.

V. NEGATIVE TRION

The process of the negative trion formation, along with the total trion energy as a function of applied lateral electric field is shown in Fig. 3. The top part shows the initial state as

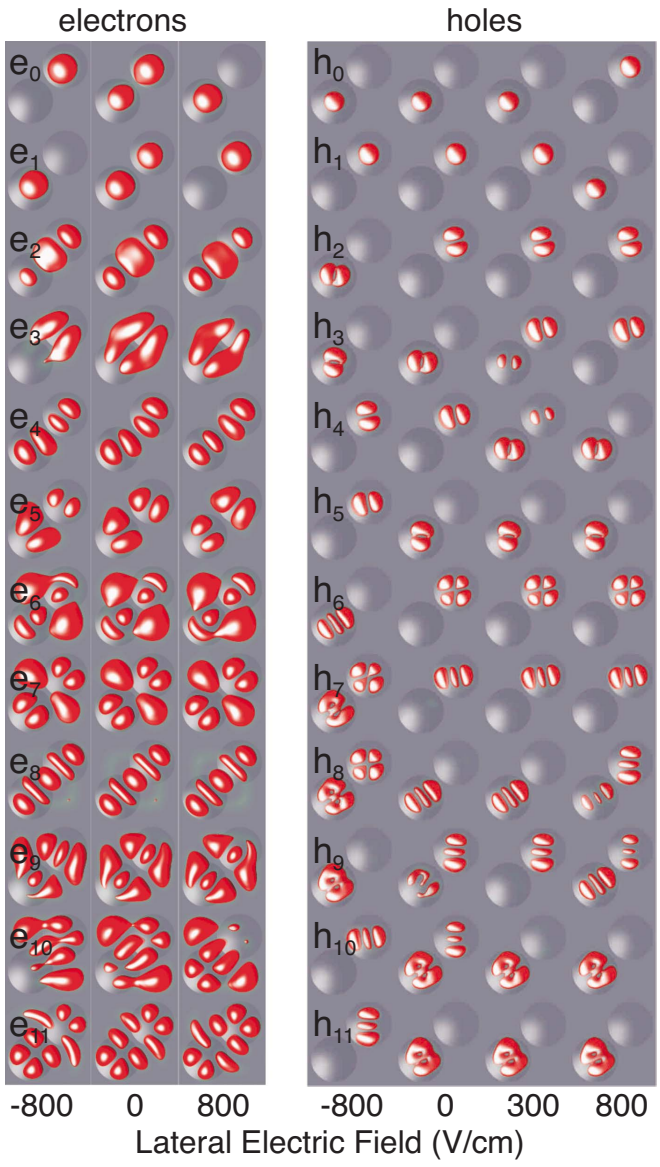

FIG. 2. (Color online) Square of the single-particle wave functions for the first 12-electron and first 12-hole states as a function of the lateral electric field. The shape of the dots is given in light gray and the dark gray (red in color) isosurfaces contain 75% of the state densities.

a single electron being in either the left of the right dot. Our understanding of the photoexcitation relies on the early capture of the electron from the hot electron-hole pair generated by nonresonant excitation.[38] In our range of fields the second electron will occupy the unoccupied dot. Only large fields, experimentally not available at the moment,[38,39] would force both electrons into the same dot. The arrival of the hole lead to LLR and RRL trions (where we use a short form with the order *hee*, see Table I). At this moment the electrons are able to redistribute between the dots, if it is energetically favorable. The lower part of the figure shows the total trion energy, which is decisive for the redistribution of electrons. The dashed lines are guides for the eyes and show the total energy in the uncoupled dot-localized basis. This is a convenient representation as it allows to follow one type of trion

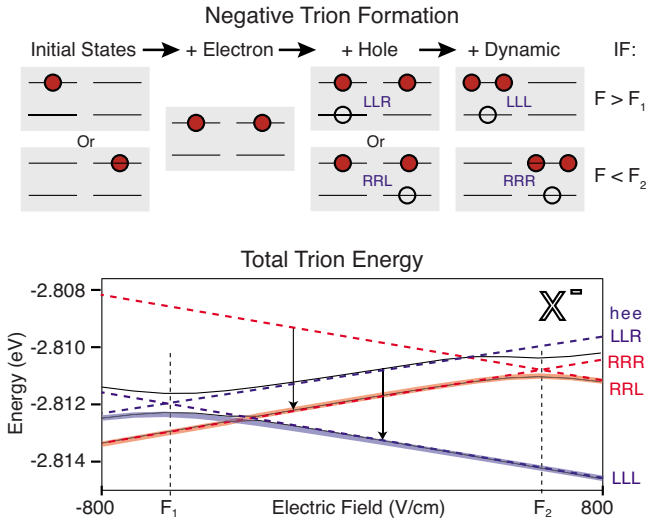

FIG. 3. (Color online) Upper panel: formation process of the negative trion for two different field situations. Lower panel: total energy of the negative trion. The allowed transitions due to electron redistribution are marked by vertical arrows.

throughout the field dependence, although the real total energy undergoes anticrossings a progressively changes character. The vertical arrows show that the RRL trion will thermalize to the RRR for fields smaller than F_2, for larger fields the total RRL trion energy is higher than the RRR energy and this process is energetically prohibited. Similarly the LLR trion thermalizes to the LLL trion for fields larger than F_1. The thick lines in Fig. 3 show the many-body levels occupied after the final step of formation. These are the levels occupied in the initial state of the photon-emission process. Note that both these levels are fully occupied and do not follow a Boltzmann distribution, due to the pinned holes. The process described is summarized in Fig. 4 along with the formation process of further charged states described subsequently.

Features due to the occupation of the initial state. The oscillator strength for the transition between the occupied trion states (Fig. 3) and the single-electron state are given in Fig. 5 as a function of the applied lateral electric field. The dashed lines are the calculated transition energies and the color map in the upper part gives the oscillator strength on a linear scale from black to white (blue to red in color). We can see several anticrossings and switching on and off of the oscillator strength with the field. The lower part of the figure analyses the results in term of the dot-localized basis, similar to the analysis of Fig. 3 but for transition energies, as opposed to total energies. Only direct exciton transitions acquire oscillator strength and these have a nearly field-independent energy. These are labeled as RRL, LLR, RRR, and LLL where we underline the recombining electron-hole pair. The higher energy RRL and LLR transitions at 1.325 eV and 1.326 eV only exist at fields larger than F_2 and smaller than F_1, respectively. This is due to the occupation of the initial trion states as a function of field, discussed previously. Only at these high and low field, the trion initial states RRL and LLR are occupied.

Features due to the anticrossings with indirect transitions.

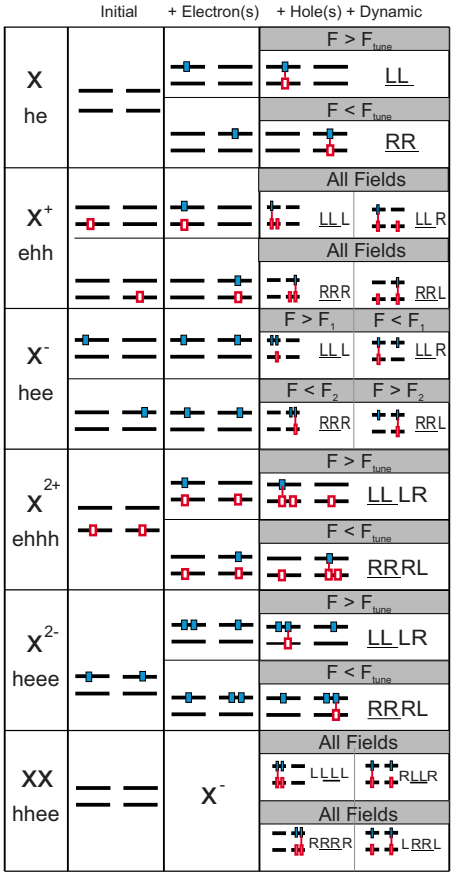

FIG. 4. (Color online) Summary of the formation processes of the different exciton complexes. The initial state in the second column is successively populated by electron(s) and holes(s) before the electrons are redistributed according to the total many-body energy of the final states.

The complex situation at intermediate fields leads to several anticrossings with indirect transitions. In Fig. 6 we analyze two of these anticrossings that originate from different types of couplings. At fields between −800 and −300 V/cm we observe an anticrossing between the transitions LLL and LRL. The transition LRL is an indirect transition and is dark. The anticrossing is due to a coupling in the initial states between the electrons. The calculated magnitude of the anticrossing is 0.76 meV and is slightly larger than the pure electron tunneling bonding-antibonding splitting of 0.66 meV. This increase can be attributed to correlations. The second anticrossing between −100 and 200 V/cm is between the transitions LLL and LLL. The transition LLL is entirely dark but still represent a valid transition process between the trion and the electron state. In this case, the coupling occurs between the final states, since the initial states are identical. The magnitude of the anticrossing is 0.66 meV in agreement with the bonding-antibonding electron splitting.

VI. POSITIVE TRION

The formation of the positive trion is described in Fig. 4. We assume that the initial hole was injected electrically and can be localized in either of the dots. The additional electron

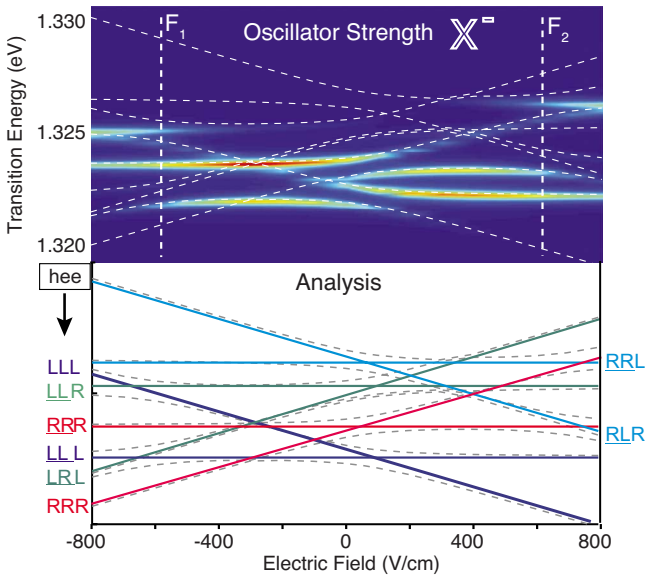

FIG. 5. (Color online) Top panel: color map of the photoluminescence intensity from the negative trion state as a function of the transition energy and the applied lateral electric field. Lower panel: analysis of the transitions, given as dotted lines in the upper panel, in the dot-localized basis.

localizes in the same dot as the resident hole, forming LL and RR excitons. The second hole can localize in any of the dots leading to four occupied X^+ states: LLL, LLR, RRR, and RRL. The total energy of these states are given in the top panel of Fig. 7. Unlike the case of the negative trion, all four states are occupied, since the holes are unable to tunnel between dots. The oscillator strength of the transitions is given in the middle panel and shows four possible transitions. The character of each is analyzed in the lower panel. The optically bright higher energy transitions 1 and 2 are LLL and RRR. These transitions are roughly separated by the difference in the single-particle gap of the left and right dots that we label Δ_{SP}. The two bright transitions 3 and 4 at lower energy are given by RRL and LLR and are roughly split by Δ_{SP} as well. The upper and lower bright states 2 and 4 are split by δ_{X^+} (Fig. 7) and can be approximated, neglecting correlations, by a difference in Coulomb integrals J as

$$\delta_{X^+} = J_{hh}^{\text{intra}} - J_{eh}^{\text{intra}} - J_{eh}^{\text{inter}}. \quad (4)$$

In Table II we summarize some Coulomb and exchange integrals for the two different structures QDM0 and QDM5. The intradot integrals are very similar for the left and right dots with difference in the range of 0.2 meV so that we report only one number. The interdot exchange integral gives the singlet-triplet splitting when both electrons are in different dots. For the dot shown in Fig. 7 (QDM5) the splitting Δ_{SP} is rather small (0.9 meV) and the splitting due to differences in Coulomb integrals in Eq. (4) is larger. In the case of QDM with larger Δ_{SP}, as for QDM0 (see Table II), the transitions 2 and 4 as well as 1 and 3, almost coincide energeti-

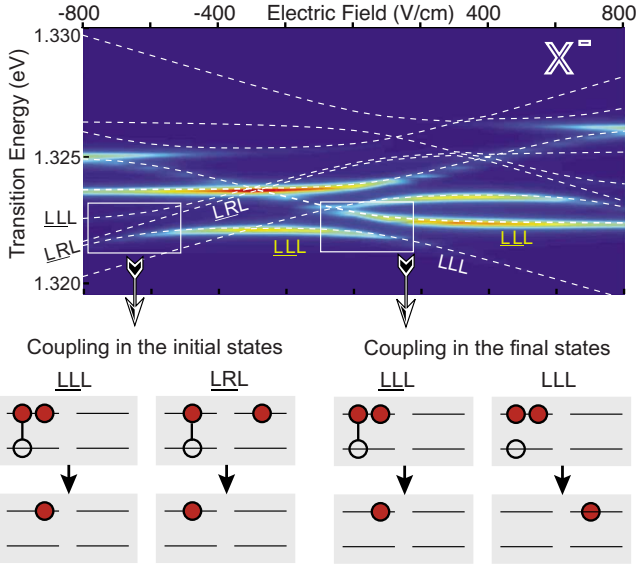

FIG. 6. (Color online) Top panel: color map of the photoluminescence intensity from the negative trion state as a function of the transition energy and the applied lateral electric field. Lower panel: analysis of the two anticrossings marked by squares in the upper panel.

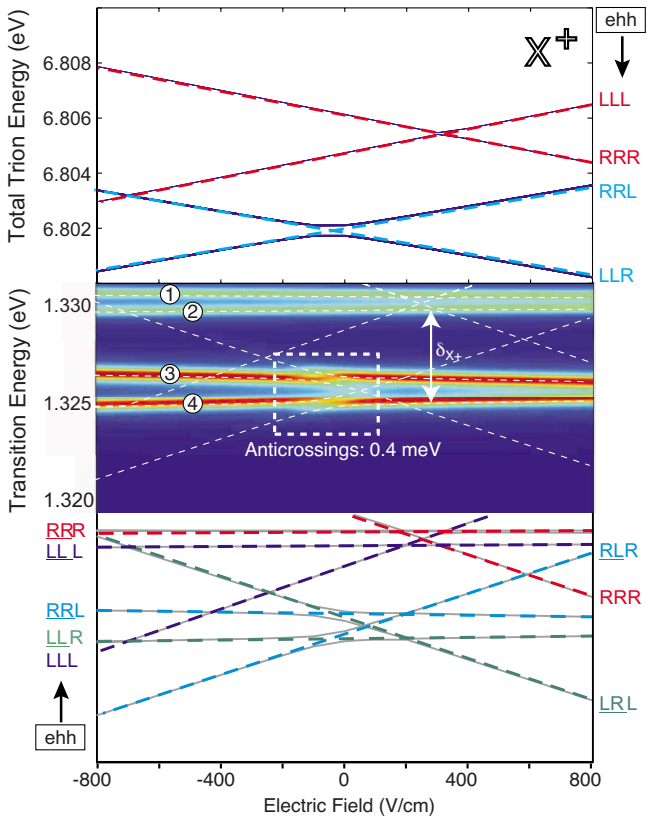

FIG. 7. (Color online) Top panel: total energy of the positive trion as a function of the applied lateral field along with the analysis of the different branches in the dot-localized basis. Middle panel: color map of the photoluminescence intensity from the positive trion state as a function of the transition energy and the applied lateral electric field. The area within the square shows two anticrossings discussed in the text. Lower panel: analysis of the transitions, given as dotted lines in the middle panel, in the dot-localized basis.

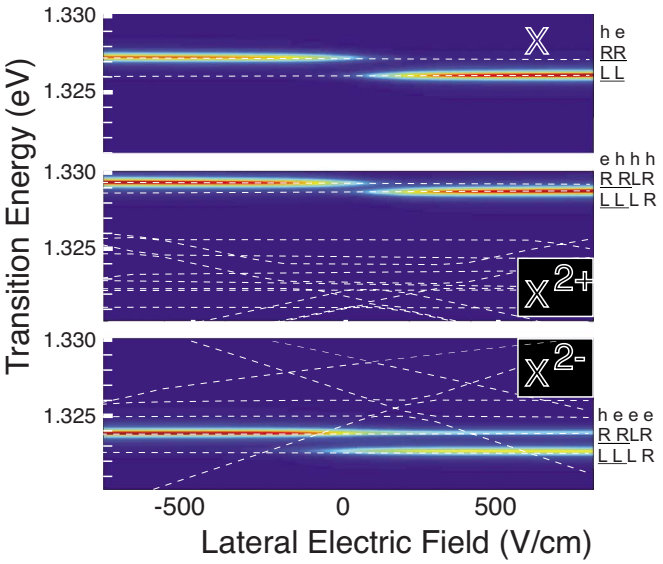

FIG. 8. (Color online) Color maps of the photoluminescence intensity from the exciton and the negative and positive quarton ($X^{2\pm}$) states as a function of the transition energy and the applied lateral electric field. The analysis of the transitions in the dot-localized basis is given in the right column.

cally. In the area marked by a square two anticrossings are present. The dark transition LRL anticrosses with the bright RRL transition 3. For the transition 4, the dark RLR anticrosses with the bright LLR transition. The magnitude of the anticrossings is 0.4 meV and is less than the bonding-antibonding splitting of the electron states.

VII. RESULTS FOR X^{2+} AND X^{2-}

The formation of X^{2+} is given in Fig. 4. We assume that the two holes occupy initially different dots. This assumption is based on the long-range Coulomb repulsion felt by the approaching second hole when entering the already occupied QDM, pushing it toward the other dot. The photogenerated electron localizes on the left or the right dot depending on the applied external field. Akin the excitonic case the threshold field is F_{tune}, when the single-particle electron states form the bonding-antibonding pair. The final hole occupies the dot where the electron is present so that the final situation is rather simple with the transition LLLR below the tuning field F_{tune} and the transition RRRL above that field. The oscillator strength as a function of the applied field is given in Fig. 8 and is very similar to the case of the exciton but shifted to higher energy.

The formation of X^{2-} is given in Fig. 4 and follows a scenario where successively three electrons enter the structure and distribute between the dots before the hole enters. The critical field which decides between the transitions LLLR and RRRL is again F_{tune}, as in the X^{2-} and the exciton case.

VIII. BIEXCITON

The transition energies of the biexciton → exciton → ground-state cascade have components from differences in Coulomb integrals and from correlation. The latter contribution being very important, sometimes dominant. In the following we will develop a qualitative model containing the relevant ingredients appearing in these transition energies and then present our quantitative results.

TABLE II. Splitting of the single-particle gap of left and right dot Δ_{SP} and Coulomb (J) and exchange integrals K in the dot localized basis for two different QDMS in millielectron volt. Our convention is to use positive values for the repulsive *ee* and *hh* integrals as well as for the attractive *eh* integrals. The signs are taken into account in the energy expressions, such as in Eq. (4). The interdot exchange term K_{ee} gives the value of the singlet-triplet splitting when two electrons occupy different dots.

		QDM5	QDM0
Intra dot	Δ_{SP}	0.9	3.2
	J_{ee}	11.2	10.6
	J_{hh}	18.9	18.4
	J_{eh}	13.2	12.6
Inter dot	J_{ee}	3.0	3.5
	J_{hh}	2.3	2.2
	J_{eh}	2.6	2.8
	K_{ee}	0.07	0.05

Neglecting correlations, the biexciton total energies can be written as a function of single-particle energies of electrons (ε^e) and holes (ε^h) and the three types of Coulomb integrals (J_{ee}, J_{hh}, and J_{eh}). Using the notation *hhee*

$$\text{LLLL} = 2(\varepsilon_e^{\text{L}} - \varepsilon_h^{\text{L}}) + J_{ee}^{\text{LL}} + J_{hh}^{\text{LL}} - 4J_{eh}^{\text{LL}},$$

$$\text{RRRR} = 2(\varepsilon_e^{\text{R}} - \varepsilon_h^{\text{R}}) + J_{ee}^{\text{RR}} + J_{hh}^{\text{RR}} - 4J_{eh}^{\text{RR}},$$

$$\text{LLRR} = (\varepsilon_e^{\text{L}} - \varepsilon_h^{\text{L}}) + (\varepsilon_e^{\text{R}} - \varepsilon_h^{\text{R}}) - J_{eh}^{\text{LL}} - J_{eh}^{\text{RR}} + J_{ee}^{\text{LR}} + J_{hh}^{\text{LR}}.$$

The first simplification is to assume the same magnitude of the intradot integrals for the left and right dots. Our calculations show differences between these in the order of 0.2 meV (18.4 meV and 18.2 meV for J_{ee}^{LL} and J_{ee}^{RR}, 12.6 meV and 12.5 meV for J_{eh}^{LL} and J_{eh}^{RR}, and 10.6 meV and 10.8 meV for J_{hh}^{LL} and J_{hh}^{RR}, respectively). With this simplification we obtain for the difference in the biexciton total energies

$$\text{LLLL} - \text{RRRR} = 2[(\varepsilon_e^{\text{L}} - \varepsilon_h^{\text{L}}) - (\varepsilon_e^{\text{R}} - \varepsilon_h^{\text{R}})] = 2\Delta_{\text{SP}}, \quad (5)$$

$$\text{LLRR} - \text{LLLL} = -\Delta_{\text{SP}} - (J_{ee} + J_{hh} - 2J_{eh}) + (J_{ee}^{\text{LR}} + J_{hh}^{\text{LR}})$$

$$= \Delta_{\text{SP}} + \delta_J,$$

where Δ_{SP} is the difference in the single-particle gap of the left and right dots. This difference can vary and is typically a few millielectron volt. The difference δ_J, that originates from a difference in the Coulomb integrals is composed of an on-site contribution ($J_{ee}+J_{hh}-2J_{eh}$) of around 3.7 meV and an off-site contribution ($J_{ee}^{\text{LR}}+J_{hh}^{\text{LR}}=3.5+2.2$ meV) of about 5.7 meV, for a total δ_J of 2 meV, in the present case. This situation is represented graphically in the upper part of Fig. 9.

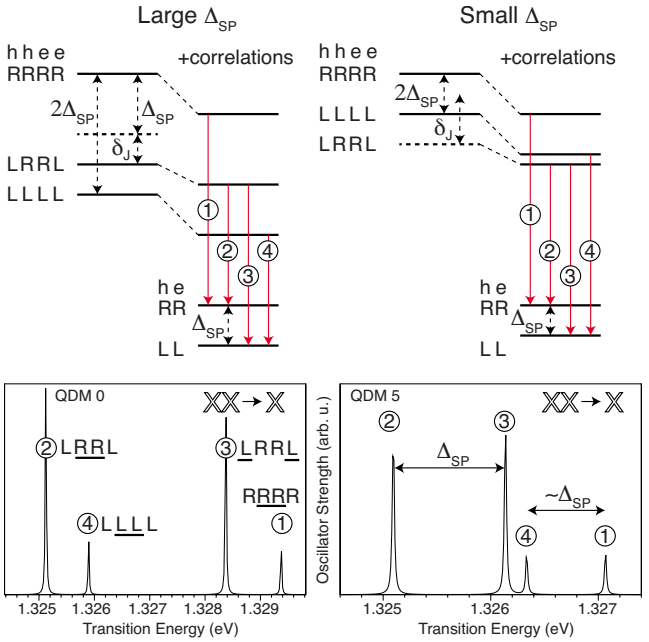

FIG. 9. (Color online) Upper panels: total energy of the lowers 18 biexciton states, where the 16 LLRR biexcitons are shown as one line. The energy splitting Δ_{SP} is the difference in the single-particle energy gap of the left and right dots. The energy shift δ_J is due to direct Coulomb interactions between the carriers see Eq. (5)] and is around 2 meV in the dots investigated. Correlations shift the segregated biexcitons (LLRR) less than the conjoined (LLLL, RRRR) ones. Lower panels: calculated oscillator strength of the emission from the biexciton states for two different QDMs. The left panel shows a QDM (QDM 0) with a rather large Δ_{SP} of 3.2 meV while the right panel shows a QDM with a small Δ_{SP} of 0.9 meV.

The effect of correlations is very important in the case of biexcitons, as it can qualitatively change the results and the energy ordering of exciton and biexciton transition energies. From a theoretical point of view great care must be taken in order to obtain converged results, i.e., include enough configurations in the configuration interaction treatment. For the present study, using six-electron and six-hole states in the expansion (4356 configuration) we obtained 4 meV correlation energy in the direct biexcitons (LLLL, RRRR). Going to the limit of our present capabilities with 12-electron and 12-hole states (76176 configurations) we obtained an additional 0.7 meV correlation energy. Going to even higher number of configurations may lower the total energy of the biexcitons somewhat further. The correlation energies we obtained are given in Table III. The correlation we obtain for the segregated biexciton, where each exciton occupies its own dot (LLRR), is smaller by roughly a factor of two compared to the correlation of a "true" conjoined biexcitons (LLLL, RRRR). This has repercussions on the total-energy level ordering, as shown in Fig. 9. Depending on the natural left-dot-right-dot difference represented by Δ_{SP}, the conjoined biexciton(s) may shift below the segregated biexciton (LLRR). The level ordering therefore depends on the separation Δ_{SP}.

The calculation of the biexciton emission is again complicated by the governing dynamical processes. The first step in the biexciton formation (see Fig. 4) is the formation of a negative trion, as previously described. After the quick thermalization of X^-, especially allowing for electron transfers, we let the last hole enter the structure to form the biexciton. Also this stage is followed by an electron transfer process, where transitions between biexciton states are allowed, when (1) the energy of the final states lies below the initial state, as in a thermalization process and (2) the holes remain localized in their respective dots, hence only the electrons can move between dots. This rather sophisticated process leads, in the biexciton case, to the simple situation that all three biexciton types: LLLL (1×), RRRR (1×), and LLRR (16×) are populated. No further relaxation of carriers is possible in these three levels, as the holes are pinned to their own dots. Even at zero temperature, the lowest three states in the QDM are occupied, a situation obviously different than in single QDs. The field dependence of the biexciton emission energy is as weak as in the case of the exciton, but the emission intensity is independent of the applied field, in contrast to the exciton case. The emission from the biexciton to the exciton is shown in Fig. 9 for the two different dot types with a large dot disparity (large Δ_{SP}, QDM0, see Table II) and a small dot disparity (small Δ_{SP}). The results shown are for 0 V/cm, but are independent of the field, within the range studied. The lower part of the figure shows the oscillator strength of the emission. Emission from the segregated biexcitons is stronger than from the conjoined exciton due to the much larger near degeneracy of the segregated type. These correspond to transitions 2 and 3 in the lower part of Fig. 9. Depending on the magnitude of the splitting Δ_{SP}, the emission can be qualitatively different with a different order of the fine-structure-rich line-3 and single-line-4.

TABLE III. Correlation energy for exciton and biexciton states. The number of configurations are given in parenthesis and refer to the configuration interaction treatment of correlations.

	Correlation energy (meV)	
Quasiparticle CI level	6 6	12 12
LLLL	4.0 (4356)	4.7 (76176)
RRRR	4.3 (4356)	5.1 (76176)
LLRR	1.8 (4356)	2.3 (76176)
LL	1.2 (144)	1.4 (576)
RR	1.0 (144)	1.4 (576)

IX. CONCLUSIONS

We have presented theoretical results for the optical properties of excitons, positive and negative trions and quartons ($X^{2\pm}$) and biexcitons. The calculations are based on million-atom empirical pseudopotential calculations and configuration interaction. We find that within the presently available range of electric fields the positive and negative trions should show anticrossings. The signature of both species is, however, very different. In the case of the negative trion we can find two anticrossings originating from a coupling of the

electrons in the final states and two anticrossings arising through coupling in the initial state. In the case of the positive trion, only two anticrossings due to coupling in the initial state are within the available field range. The magnitude of the anticrossings are shown to vary depending on the type of coupling. In the case of the final-state coupling, where only a single electron occupies the structure leads to an anticrossing of 0.66 meV, which is simply the bonding-antibonding splitting of the single-particle states. In the case of an initial state tunneling between many-body trion states the anticrossing changes to 0.76 meV in the case of X^- and 0.40 meV for X^+. These variations are many-body effects on tunneling that should be experimentally observable in the near future. For the biexciton we predict two weak and two strong transitions, mainly independent of the applied field (in the range of presently available fields). We provide a simple model for the spacing and ordering of the peaks that should be usable for a wide range of lateral QDMs.

*g.bester@fkf.mpg.de

[1] *Lateral Alignment of Epitaxial Quantum Dots*, edited by O. G. Schmidt (Springer, New York, 2007).

[2] L. Wang *et al.*, New J. Phys. **10**, 045010 (2008).

[3] N. Bonadeo, J. Erland, D. Gammon, D. Park, D. Katzer, and D. Steel, Science **282**, 1473 (1998).

[4] T. H. Stievater, X. Li, D. G. Steel, D. Gammon, D. S. Katzer, D. Park, C. Piermarocchi, and L. J. Sham, Phys. Rev. Lett. **87**, 133603 (2001).

[5] H. Kamada, H. Gotoh, J. Temmyo, T. Takagahara, and H. Ando, Phys. Rev. Lett. **87**, 246401 (2001).

[6] H. Htoon, T. Takagahara, D. Kulik, O. Baklenov, A. L. Holmes, and C. K. Shih, Phys. Rev. Lett. **88**, 087401 (2002).

[7] A. Zrenner, E. Beham, S. Stufler, F. Findeis, M. Bichler, and G. Abstreiter, Nature (London) **418**, 612 (2002).

[8] X. Li, Y. Wu, D. Steel, D. Gammon, T. H. Stievater, D. S. Katzer, D. Park, C. Piermarocchi, and L. J. Sham, Science **301**, 809 (2003).

[9] M. Atatüre, J. Dreiser, A. Badolato, A. Högele, K. Karrai, and A. Imamoglu, Science **312**, 551 (2006).

[10] X. Xu, Y. Wu, B. Sun, Q. Huang, J. Cheng, D. G. Steel, A. S. Bracker, D. Gammon, C. Emary, and L. J. Sham, Phys. Rev. Lett. **99**, 097401 (2007).

[11] D. Kim, S. E. Economou, Ş. C. Bădescu, M. Scheibner, A. S. Bracker, M. Bashkansky, T. L. Reinecke, and D. Gammon, Phys. Rev. Lett. **101**, 236804 (2008).

[12] J. Berezovsky, M. H. Mikkelsen, N. G. Stoltz, L. A. Coldren, and D. D. Awschalom, Science **320**, 349 (2008).

[13] A. J. Ramsay, S. J. Boyle, R. S. Kolodka, J. B. B. Oliveira, J. Skiba-Szymanska, H. Y. Liu, M. Hopkinson, A. M. Fox, and M. S. Skolnick, Phys. Rev. Lett. **100**, 197401 (2008).

[14] D. Press, T. D. Ladd, B. Zhang, and Y. Yamamoto, Nature (London) **456**, 218 (2008).

[15] A. Greilich, S. E. Economou, S. Spatzek, D. R. Yakovlev, D. Reuter, A. D. Wieck, T. L. Reinecke, and M. Bayer, Nat. Phys. **5**, 262 (2009).

[16] E. D. Kim, K. Truex, X. Xu, B. Sun, D. G. Steel, A. S. Bracker, D. Gammon, and L. J. Sham, Phys. Rev. Lett. **104**, 167401 (2010).

[17] Q. H. Xie, A. Madhukar, P. Chen, and N. P. Kobayashi, Phys. Rev. Lett. **75**, 2542 (1995).

[18] G. S. Solomon, J. A. Trezza, A. F. Marshall, and J. S. Harris, Phys. Rev. Lett. **76**, 952 (1996).

[19] G. Schedelbeck, W. Wegscheider, M. Bichler, and G. Abstreiter, Science **278**, 1792 (1997).

[20] A. S. Bracker, M. Scheibner, M. F. Doty, E. A. Stinaff, I. V. Ponomarev, J. C. Kim, L. J. Whitman, T. L. Reinecke, and D. Gammon, Appl. Phys. Lett. **89**, 233110 (2006).

[21] H. J. Krenner, M. Sabathil, E. C. Clark, A. Kress, D. Schuh, M. Bichler, G. Abstreiter, and J. J. Finley, Phys. Rev. Lett. **94**, 057402 (2005).

[22] G. Ortner, M. Bayer, Y. Lyanda-Geller, T. L. Reinecke, A. Kress, J. P. Reithmaier, and A. Forchel, Phys. Rev. Lett. **94**, 157401 (2005).

[23] E. Stinaff, M. Scheibner, A. Bracker, I. Ponomarev, V. Korenev, M. Ware, M. Doty, T. Reinecke, and D. Gammon, Science **311**, 636 (2006).

[24] L. Robledo, J. Elzerman, G. Jundt, M. Atature, A. Hoegele, S. Faelt, and A. Imamoglu, Science **320**, 772 (2008).

[25] G. Bester, J. Shumway, and A. Zunger, Phys. Rev. Lett. **93**, 047401 (2004).

[26] L. X. He, G. Bester, and A. Zunger, Phys. Rev. B **72**, 195307 (2005).

[27] W. Jaskólski, M. Zieliński, G. W. Bryant, and J. Aizpurua, Phys. Rev. B **74**, 195339 (2006).

[28] G. Bester, A. Zunger, and J. Shumway, Phys. Rev. B **71**, 075325 (2005).

[29] M. F. Doty, J. I. Climente, M. Korkusinski, M. Scheibner, A. S. Bracker, P. Hawrylak, and D. Gammon, Phys. Rev. Lett. **102**, 047401 (2009).

[30] M. F. Doty, J. I. Climente, A. Greilich, M. Yakes, A. S. Bracker, and D. Gammon, Phys. Rev. B **81**, 035308 (2010).

[31] M. Garrido, K. C. Wijesundara, S. Ramanathan, E. A. Stinaff, A. S. Bracker, and D. Gammon, Appl. Phys. Lett. **96**, 211115 (2010).

[32] D. Kim, S. Carter, A. Greilich, A. Bracker, and D. Gammon, arXiv:1007.3733 (unpublished).

[33] Z. Wang, C. Rodriguez, S. Seydmohamadi, Y. Mazur, Y. Xie, and G. Salamo, Appl. Phys. Lett. **94**, 083107 (2009).

[34] L. Wang, A. Rastelli, S. Kiravittaya, M. Benyoucef, and O. G. Schmidt, Adv. Mater. **21**, 2601 (2009).

[35] Z. M. Wang, K. Holmes, Y. I. Mazur, K. A. Ramsey, and G. J. Salamo, Nanoscale Res. Lett. **1**, 57 (2006).

[36] J. H. Lee, Z. M. Wang, N. W. Strom, Y. I. Mazur, and G. J. Salamo, Appl. Phys. Lett. **89**, 202101 (2006).

[37] G. J. Beirne, C. Hermannstädter, L. Wang, A. Rastelli, O. G. Schmidt, and P. Michler, Phys. Rev. Lett. **96**, 137401 (2006).

[38] J. Peng, C. Hermannstädter, M. Witzany, M. Heldmaier, L. Wang, S. Kiravittaya, A. Rastelli, O. G. Schmidt, P. Michler, and G. Bester, Phys. Rev. B **81**, 205315 (2010).

[39] C. Hermannstadter, G. J. Beirne, M. Witzany, M. Heldmaier, J. Peng, G. Bester, L. Wang, A. Rastelli, O. G. Schmidt, and P.

Michler, Phys. Rev. B **82**, 085309 (2010).
[40] M. Heldmaier *et al.*, Phys. Rev. B (to be published).
[41] R. Songmuang, S. Kiravittaya, and O. G. Schmidt, Appl. Phys. Lett. **82**, 2892 (2003).
[42] L.-W. Wang and A. Zunger, Phys. Rev. B **59**, 15806 (1999).
[43] G. Bester, J. Phys.: Condens. Matter **21**, 023202 (2009).
[44] A. Franceschetti, H. Fu, L.-W. Wang, and A. Zunger, Phys. Rev. B **60**, 1819 (1999).
[45] G. Bester, S. Nair, and A. Zunger, Phys. Rev. B **67**, 161306(R) (2003).